High power red laser generation by second harmonic generation with GTR-KTP crystal

Baitao Zhang (张百涛)*, Jian Ning (宁 建), Zhaowei Wang (王兆伟), Kezhen Han (韩克祯), and Jingliang He (何京良)

State Key Laboratory of Crystal Materials, Shandong University, Jinan 250100, China
**Corresponding author: bai3697@126.com*

Received January 23, 2015; accepted March 16, 2015; posted online April 24, 2015

In this Letter, a gray-tracking-resistant—potassium titanyl phosphate (GTR-KTP) crystal is used for intracavity frequency doubling red laser generation for the first time. Under the 808 nm LD pump power of 180 W, as high as 12.5 W of red laser output is obtained with the optimum repetition rate of 7 kHz. Within the red laser power variation range between the maximum to 70%, a temperature tolerance is measured to be 35°C. The results prove that GTR-KTP should be a potential nonlinear crystal for red laser generation.

OCIS Codes: 140.3515, 140.3480, 140.3580.
doi: 10.3788/COL201513.051402.

Potassium titanyl phosphate ($KTiOPO_4$, KTP) is widely used for second harmonic generation (SHG) and optical parametric oscillations (OPOs) because of its high effective nonlinear coefficient, large acceptance angle, and large temperature bandwidth[1–4]. However, the laser induced damage gray-tracking problem limits the lifetime of KTP crystals for high-average-power SHG, especially for green laser generation[5–7]. The formation and absorption of Ti^{3+} and Fe^{3+} centers generated in KTP crystals give rise to the gray-tracking effect[8]. As a pyroelectric crystal, a dc electric field generated under the heating effect induced by the laser beam radiation makes electrons and holes drift toward the $+z$ and $-z$ directions. As a consequence, the electrons should be trapped in the Ti^{4+} ions located adjacent to the OH^- ions or oxygen vacations, creating Ti^{3+} centers on the $+z$ side. Meanwhile, the holes should be trapped in impurities such as Fe^{2+} to create Fe^{3+} ions. Optical absorption bands associated with these electron and hole traps give rise to the gray-tracking color[9]. The optical properties of KTP crystals depend greatly on their structural characteristics, such as morphology, chemical composition, and defect distribution, which are closely related to the specific crystal growth parameters. Optimizing the crystal growth conditions and adopting highly purified raw materials can improve the resistance of KTP crystals to gray-tracking effects[10–13].

Tens of watts levels of high power red lasers have wide applications in the fields such as medical treatment, laser color display, high resolution laser printing, and pumping sources such as Cr:LiSAF lasers[14]. The frequency doubling of 1.3 μm diode pumped solid state lasers (DPLs) with nonlinear crystals is an effective method for generating high power red lasers[15–18]. Compared with the red laser diodes, DPL red lasers have many advantages such as high beam quality, narrow line width, and small divergence. LiB_3O_5 is one of the most promising candidates especially for high-average-power SHG owing to high damage thresholds. However, its effective nonlinear coefficient (0.65 pm/V) is approximately 1/5 of that of KTP (3.13 pm/V), which limits its SHG conversion efficiency. Many studies have proven that improving resistance to the gray-tracking effect can be favorable for obtaining high efficient and high power 532 nm generations[19,20]. The absorption coefficients of a 633 nm red laser for gray-tracking-resistant (GTR)-KTP and conventional KTP (C-KTP) are 0.1×10^{-4} and 2.75×10^{-4} cm^{-1}, respectively[21], which indicates that GTR-KTP should be a potential nonlinear crystal used for SHG red laser generation instead of C-KTP. However, there are no reports about the characteristics of GTR-KTP crystals used for SHG red laser generation.

In this Letter, based on a GTR-KTP crystal, an intracavity frequency-doubling red laser is demonstrated. The maximum red laser output power of 12.5 W is generated with optical-optical conversion efficiencies of 6.9%, which are higher than that obtained with C-KTP under the same situation (9.2 W and 5.1%). What is more, a temperature tolerance of GTR-KTP is measured to be 35°C, which is broader than the 24°C with C-KTP. The results indicate that GTR-KTP should be a potential nonlinear crystal used for 1.3 μm laser frequency doubling.

The experimental configuration is shown in Fig. 1. A Nd:YAG laser module in which a water-cooled Nd:YAG rod (1 at.%) with the dimensions of $\Phi 3 \times 65$ (mm) is side-pumped by nine CW diode arrays with an available maximum output power of approximately 180 W at 808 nm, is employed. The Nd:YAG crystal was cooled with circulating water at 23°C during the experiments.

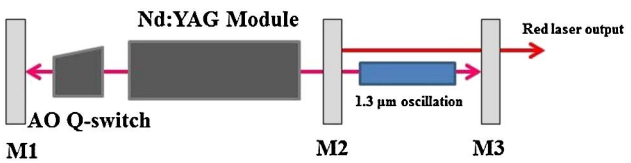

Fig. 1. Schematic diagram of the intracavity SHG red laser.

The surface temperature of the Nd:YAG crystal is kept at about 23°C during the experiments. The 1.3 μm fundamental cavity is made up of a rear mirror M1, the Nd:YAG module, an acousto-optical (AO) Q-switch, and an end mirror M3. M1 is a concave mirror with an 800 mm radius of curvature and high-reflection (HR) coated at 1331 nm (R > 99.8%). The AO Q-switch has antireflection (AR) coatings at 1331 nm on both surfaces and is driven at a 40.06 MHz center frequency with 50 W of radio frequency (RF) power. The red laser cavity consists of an internal flat mirror M2, a KTP crystal for SHG, and the end mirror M3. M2 is AR coated at 1331 nm (R < 0.2%) on surface S1, high transmission (HT)-coated at 1331 nm (T > 98%), and HR-coated at 665 nm (R > 99%) on the other surface S2. M3 functions as the output coupler for 665 nm with HT-coated at 665 nm and HR-coated at 1331 nm. The 1.3 μm oscillation was established between M1 and M3, and the SHG would be enhanced between M2 and M3. The GTR-KTP and C-KTP crystals are both cut into $4 \times 4 \times 10$ (mm) with type II phase matching ($\theta = 59.5°$ and $\phi = 0°$) at 1331 nm. Both crystals are AR-coated at 1331 and 665 nm (R < 0.2%) on both surfaces to minimize the internal losses caused by the Fresnel reflection. The two nonlinear crystals were wrapped with indium foil and mounted in an oven with a temperature accuracy of ±0.1°C. The overall length of the fundamental cavity is 190 mm, and the red laser cavity length is determined to be 25 mm. The average output power was recorded by a laser power meter behind the filter that was used to eliminate the effect of the 1.3 μm radiation. The temporal shape of the output laser pulse was recorded by a Tektronix DPO7104 digital oscilloscope (1 GHz bandwidth, 5 Gs/s sampling rate) and a photodetector (New Focus, model 1621).

Without a KTP crystal in the cavity, the maximum output power of 1.3 μm is measured to be 22.5 W under the maximum pump power of 180 W when an output coupler with transmittance of T = 8% at 1.3 μm is used. The corresponding optical-optical conversion efficiency is 12.5%. Then, putting the KTP crystal between M2 and M3, we obtained the red laser output. There are two strong transitions in the 1.3 μm region for the Nd:YAG laser; one is the R2 → X1 transition at 1319 nm and the other is the R2 → X3 transition at 1338 nm. The effective stimulated emission cross sections for both transitions are almost the same: 0.95×10^{-19} and 1.0×10^{-19} cm^2[22]. The two transitions always existed at the same time. What is more, the KTP crystals used for the SHG in the experiment have a large mix acceptance bandwidth (115.05 cm$^{-1}\cdot$cm). Therefore, there are three emission peaks of the red laser: the peak at 659.5 nm is obtained by frequency doubling of the transition at 1319 nm and the peak at 669 nm is obtained by frequency doubling of the transition at 1338 nm, while the 664.2 nm peak is generated by sum-frequency between the transitions at 1319 and 1338 nm.

With the LD pump power fixed at 130 W, we change the AO Q-switch repetition rates to investigate the variation of the red laser output power, as is shown in Fig. 2. The variation of the red laser output power versus the repetition rates can be understood as follows. For a given cavity and LD pump power, increasing the repetition rate, the number of fundamental pulses per second will be increased, but the corresponding single pulse peak power decreases. At the beginning, the number increase of the fundamental pulses should dominate the SHG performance, so the average red laser output power increased first. Then, decrease of the single pulse peak power caused by a further increase of the fundamental pulses gradually becomes the stronger process. This could contribute to the decrease of the red laser output power with a high repetition rate. Therefore, there should be an optimum repetition rate for obtaining the maximum red laser output power under a given pump power. According to Fig. 2, the optimal repetition rate in our experiment was measured to be 7 kHz for the maximum average red output power and the SHG conversion efficiency obtained with GTR-KTP was higher than that obtained with C-KTP.

The dependence of the normalized SHG red laser output power on temperature was performed under the LD pump power of 130 W and the repetition rate of 7 kHz. The corresponding results for GTR-KTP and C-KTP are shown in Fig. 3(a) and Fig. 3(b), respectively. In order to prevent condensation, the initial testing temperature was set to be 15°C. As can be seen from Fig. 3, the normalized red laser output power fluctuated in the range from 0.75 to 1.0 during the temperature increased from 15 to 50°C. When the temperature exceeded 50°C, the output power decreased sharply. This should be attributed to the subsequent thermal dephasing under high temperature. From the results we obtained for the 532 nm SHG in Ref. [19], the output power would present a periodic variation when the temperature exceeded some value. In our experiment, the higher temperature is set to be 55°C for the oven controller problem. For C-KTP, in the normalized output power range from 0.75 to 1.0, the temperature scope

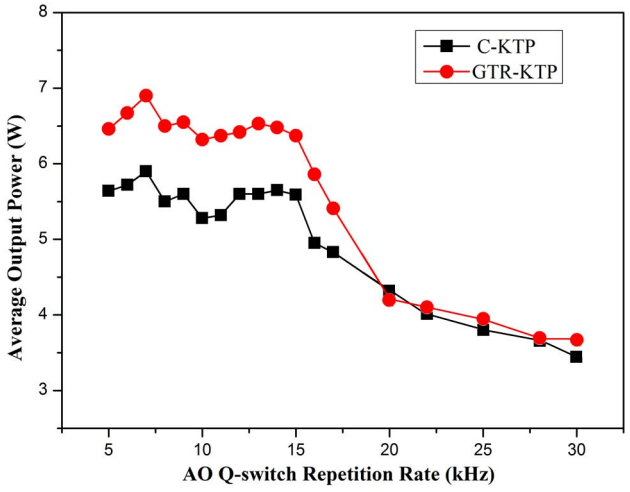

Fig. 2. Average red output power versus repetition rates for two KTP crystals under the LD pump power of 130 W.

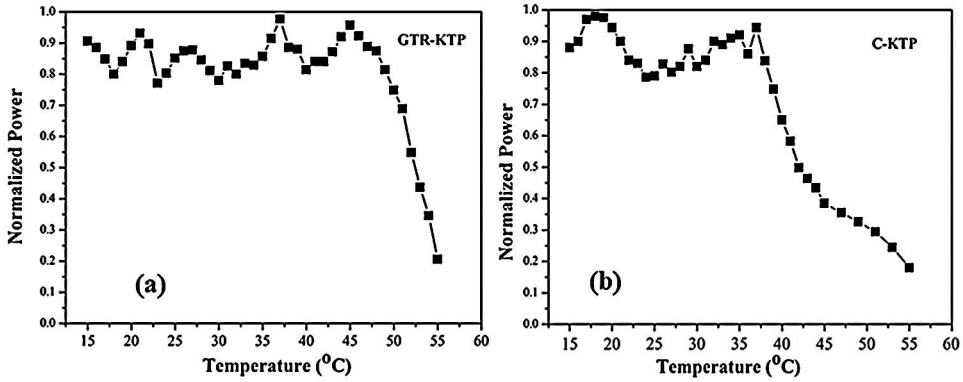

Fig. 3. Temperature tuning curve for the intracavity SHG crystals: (a) for GTR-KTP with a temperature range of 15–50°C; (b) for C-KTP with a temperature range of 15–39°C.

was determined to be 24°C with temperature increasing from 15 to 39°C. The temperature range obtained in our experiment exceeded the temperature bandwidth for KTP type-II phase matching at 1.3 μm. Therefore, the temperature tolerance introduced here was to characterize this temperature insensitivity obtained with the intracavity KTP crystals to avoid confusion with the defined temperature phase-matching bandwidth. Apparently, the GTR-KTP crystal had a higher temperature tolerance (35°C) than that of C-KTP (24°C). The higher temperature tolerance may be used in some military applications.

According to Fig. 3, the temperatures of the GTR-KTP and C-KTP were set at 21 and 19°C, respectively. The average red laser output power was measured with an AO Q-switch repetition rate of 7 kHz and the results are shown in Fig. 4. Under the maximum pump power of 180 W, the highest red output power of 12.5 W was obtained for GTR-KTP with the optical-optical conversion efficiency of 6.9%, which is higher than that obtained by LBO crystals we ever demonstrated (12 W, 6.6% for 15 mm-long type I phase matching, and 10.6 W, 5.8% for 12 mm-long type II phase matching). For C-KTP, the corresponding maximum red average output power was measured to be 9.2 W. The red laser conversion efficiency for GTR-KTP was always higher than that for C-KTP. Figure 5 shows the variation of red laser pulse widths versus the LD pump power at the repetition rate of 7 kHz. The pulse duration decreased according to the augment of the pump power because increasing the pump power resulted in an increase of the atom number pumped into the upper laser level per second and unit volume in Nd:YAG. With the pump power increasing from 30 to 180 W, the pulse durations decreased from 276.8 to 120.6 ns for C-KTP, while they varied from 345.7 to 88.9 ns for GTR-KTP. The maximum single-pulse energy and peak power could be estimated to be 1.79 mJ and 14.8 kW for the 12.5 W red output power obtained in the case of GTR-KTP. The power instability at the maximum output power of 12.5 W is observed to be less than 3.4% during one hour. The corresponding beam quality factor M^2 is measured to be 10.5 ± 1 by the knife-edge method, which is better than the case of C-KTP (M^2 is measured to be

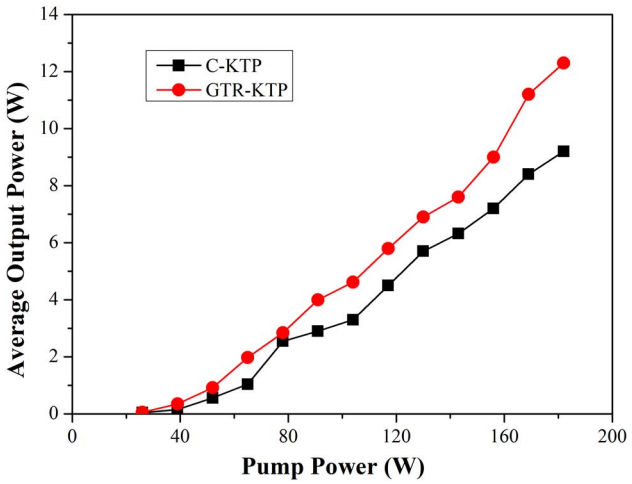

Fig. 4. Intracavity SHG red laser output power versus the LD pump power when the temperatures of the GTR-KTP and C-KTP were set at 21 and 19°C, respectively.

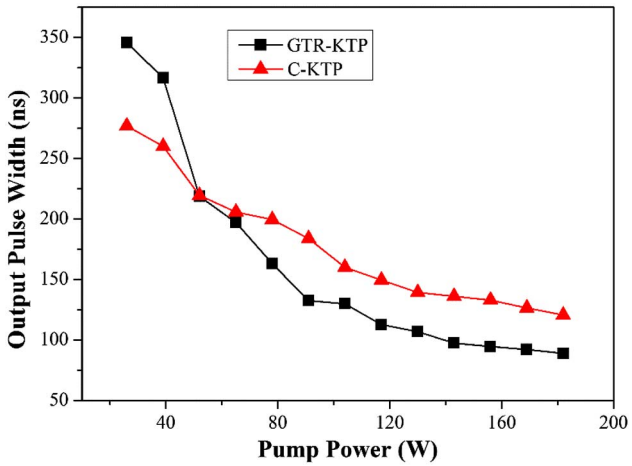

Fig. 5. Variations of red laser pulse widths versus the LD pump power for GTR-KTP and C-KTP at the repetition rate of 7 kHz.

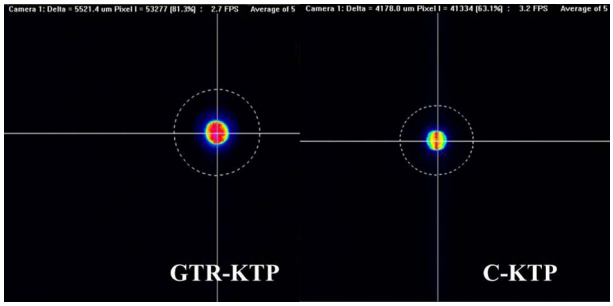

Fig. 6. Beam profiles of the red laser obtained with the two crystals.

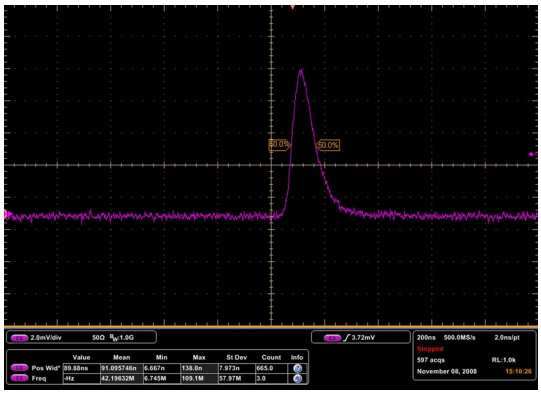

Fig. 7. Temporal pulse shape of the red laser obtained by the C-KTP crystal.

11.4 ± 1). The beam profiles of the red laser obtained with the two crystals are shown in Fig. 6. Due to the aggravated thermal effect in C-KTP, the spatial mode is asymmetric. Figure 7 shows the minimum temporal pulse shape of the red laser obtained by the GTR-KTP crystal.

In conclusion, an intracavity frequency-doubling red laser with GTR-KTP is demonstrated for the first time to our knowledge. The C-KTP crystal is used under the same condition for comparison. Like that used for 1.06 μm SHG, GTR-KTP has a broader temperature tolerance than C-KTP (35 vs. 24°C) when they are used for 1.3 μm SHG. The maximum red output power of 12.5 W is obtained with GTR-KTP, while it is 9.2 W with C-KTP under the same condition. The results indicate that GTR-KTP should be a potential nonlinear crystal for red laser generation.

This work was supported by the National Natural Science Foundation of China (Grant Nos. 61308042 and 61275142), and the China Postdoctoral Science Foundation (Grant Nos. 2013M531594 and 2014T70633).

References

1. D. Eimerl, IEEE J. Quantum Electron. **23**, 1361 (1987).
2. B. Jiao, J. Tian, X. Zhang, Y. Song, and L. Wang, Chin. Opt. Lett. **11**, S21901 (2013).
3. H. Zhang, Y. Zhang, X. Tan, Y. Geng, K. Zhong, X. Li, P. Wang, and J. Yao, Chin. Opt. Lett. **07**, 802 (2009).
4. Y. Jiang, H. Liu, L. Wang, C. Jiang, Y. Ji, and Y. Yang, Chin. Opt. Lett. **11**, S10406 (2013).
5. H. Kiriyama, S. Matsuoka, Y. Maruyama, and T. Arisawa, Opt. Commun. **174**, 499 (2000).
6. N. B. Angert, V. M. Garmash, N. I. Pavlova, and A. V. Tarasov, IEEE J. Quantum Electron. **21**, 426 (1991).
7. L.-X. Zou, Y.-Z. Huang, X.-M. Lv, B.-W. Liu, H. Long, Y.-D. Yang, J.-L. Xiao, and Y. Du, Photon. Res. **2**, 177 (2014).
8. B. Boulanger, I. Rousseau, J. Feve, M. Maglione, B. Menaert, and G. Marnier, IEEE J. Quantum Electron. **35**, 281 (1999).
9. X. Mu and Y. J. Ding, Appl. Opt. **39**, 3099 (2000).
10. L. E. Halliburton and M. P. Scripsick, Proc. SPIE **2379**, 235 (1995).
11. M. P. Scripsick, D. N. Loiacono, J. Rottenberg, S. H. Goellner, L. E. Halliburton, and F. K. Hopkins, Appl. Phys. Lett. **66**, 3428 (1995).
12. L. Ji, B. Zhu, C. Liu, T. Wang, and Z. Lin, Chin. Opt. Lett. **12**, 031902 (2014).
13. G. M. Loiacono, D. N. Loiacono, T. McGee, and M. Babb, J. Appl. Phys. **72**, 2705 (1992).
14. P. M. W. French, P. J. Delfyett, L. T. Florez, R. Mellish, and J. Taylor, Opt. Lett. **18**, 1934 (1993).
15. C. Du, S. Ruan, Y. Yu, and F. Zeng, Opt. Express **13**, 2013 (2005).
16. W. Qin, C. Du, S. Ruan, and Y. Wang, Opt. Express **15**, 1594 (2007).
17. X. P. Hu, P. Xu, and S. N. Zhu, Photon. Res. **1**, 171 (2013).
18. L. Wang, Y. Chen, and G. Liu, Chin. Opt. Lett. **12**, 111902 (2014).
19. J. P. Feve, B. Boulanger, G. Marnier, and H. Albrecht, Appl. Phys. Lett. **70**, 277 (1997).
20. H.-T. Huang, G. Qiu, B.-T. Zhang, J.-L. He, J.-F. Yang, and J.-L. Xu, Appl. Opt. **48**, 6371 (2009).
21. S. Rongbing, C. Yu, C. Lina, C. Jinfeng, Z. Wenrong, and Z. Jian, J. Synth. Cryst. **37**, 104 (2008).
22. A. A. Kaminskii, "Luminescence and stimulated-emission properties of laser crystals in the Y_2O_3–Al_2O_3 system," in *Laser Crystals* (Springer, 1990), p. 319.